



PROJECT A12 FINAL REPORT

Stefania Caragnano, University of Bari, Italy

September 02, 2021

Abstract

In the attosecond science and technology group at CFEL ultrashort laser pulses with attosecond or few-femtosecond duration are generated. They are used to trigger photoreactions in and to follow in real-time how the atoms and electrons move and interact. This project has been divided into three parts.

The first one consisted of analysing the provided data regarding a XUV attosecond pulse train in order to calibrate an XUV spectrometer. In particular, the pulse interacted with an aluminum filter. It was the obtained fundamental frequency (photon energy) from the spectrum of driving infrared laser and then a physical model to relate image coordinate (pixels) to photon energy has been elaborate. Finally, after making the calibration, the spectrum has been converted into a calibrated graph with photon energy on the abscissa axis.

Then, the second part of the project was dedicated to the analysis of provided data regarding different ionized samples in order to recognize them and their component molecules using mass spectra.

In conclusion, the third and last part of the project was about calibrating an electron spectrometer and the analysis of VMI (velocity map imaging) data. The main aim of this part was to elaborate images from the given data in order to obtain informations about the kinetic energy of the detected electrons after the ionization of chosen samples using different kind of lights. These images were also used to come to other conclusions about the experimental process.

Contents

1. Photon Spectrometer Calibration.....	3
1.1 Introduction.....	3
1.2 Data Analysis.....	4
2. Mass Spectrometry.....	8
2.1 Introduction.....	8
2.2 Data Analysis.....	9
3. Velocity Map Imaging (VMI) Spectroscopy.....	12
3.1 Introduction.....	12
3.2 Data Analysis.....	12
4. Conclusions for the experience.....	14
5. Appendix.....	15
6. References.....	16

1. Photon Spectrometer Calibration

1.1 Introduction

High harmonic generation

When an intense and short laser pulse is focused into a gas medium, the electronic response becomes highly nonlinear and high-order harmonics of the driving laser frequency can be generated.

Only odd harmonics of the fundamental frequency are generated for reasons of symmetry. Indeed, in a gas target a reversal of the driving field must cause a reversal of the nonlinear polarization, which is the source of the harmonic emission.

Depending on the intensity and wavelength of the driving field, the spectrum of this burst of photons may extend in the EUV (extreme ultra violet) from a few electronvolts to a few hundreds of electronvolts. [1]

Spectral separation produced by diffraction grating

Below is shown a diagram of the internal structure of the spectrometer that was used for this experiment.

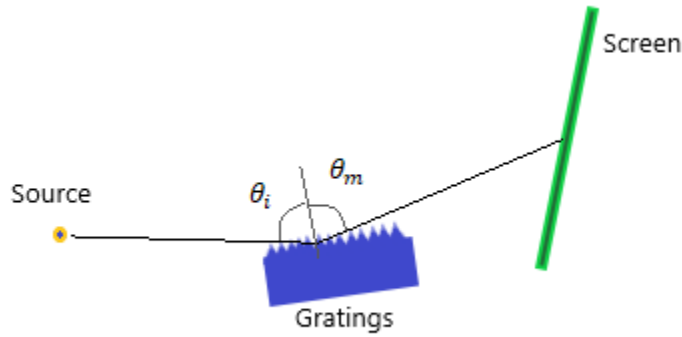


Figure 1

This device contained a diffraction grating by reflection which was hit by the electromagnetic radiation. The radiation then was diffracted and detected by a camera placed immediately after the grating. The output images were recorded as intensity values as a function of the pixel position on the camera. In order to find the position of the maximum intensity values on the screen, the following relationship must be used:

$$d \sin \theta_i - d \sin \theta_m = m \lambda \quad (1)$$

where d is the line spacing and θ_i is the incident, m is the order, θ_m is the angle under which the order m is identified on the screen and λ is the wavelength of the incident radiation.

Moreover

$$\tan \theta_m = \frac{L}{y} \quad (2)$$

Where L is the distance between the grating and the screen and y the position of the peaks on the screen.

By replacing (2) in (1) and calling $A = d \sin \theta_i$ we obtain the relationship used later for data analysis:

$$y = \frac{L}{\tan(\arcsin\left(\left(\frac{1}{d}\right)\left(A - \frac{mhc}{E}\right)\right))} \quad (3)$$

where was also used

$$\lambda = \frac{hc}{E} \quad (4)$$

E is the photon energy.

The complete calculations are reported into the appendix (II).

Definition of transmittance

When a light beam interacts with a sample of known material, depending on the characteristics of the latter, this beam will be transmitted beyond the obstacle with different percentages depending on the energy it possesses.

The transmittance through an object can be defined as

$$T(E) = \frac{I_o(E)}{I_i(E)} \quad (5)$$

where in the numerator is the intensity of the light beam exiting the material and in the denominator the input intensity. By definition, therefore, this magnitude is a percentage linked to the energy of the light pulse.

The experimental apparatus consists of two arms, as shown in figure 1.

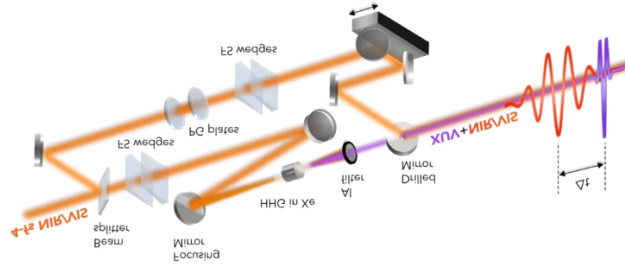


Figure 2: exemplary model of the experimental setup. (E. Månsson, Lecture for DESY Summer Student Program 2021 (personal communication))[2].

1.2 Data Analysis

The graphs obtained are shown below.

The fundamental frequency ω_0 and photon energy E_0 were determined by taking the peak value of the spectrum of the IR pulse.

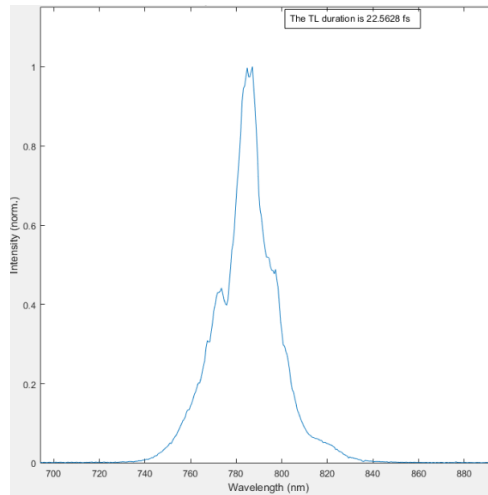


Figure 3: spectrum of the IR pulse. (E. Månsson, Lecture for DESY Summer Student Program 2021 (personal communication))[2].

The relationships used were the following:

$$E_0 = \frac{h\omega_0}{e} \quad (6)$$

Where energy is calculated in eV, h is Planck's constant and e the electron charge.

While, for the wavelength

$$\lambda_0 = \frac{2\pi c}{\omega_0} = \frac{c}{f_0} \quad (7)$$

where c is the speed of light.

And so

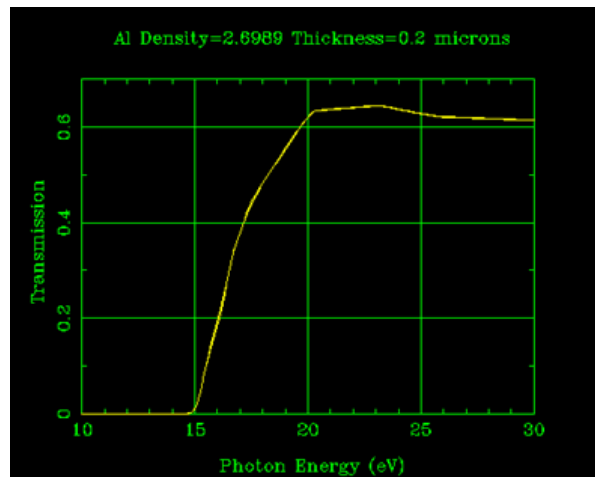
$$f_0 = \frac{c}{\lambda_0} \quad (8)$$

The recorded values were used to calculate the transmittances corresponding to each peak and therefore to each harmonic order of the pulse.

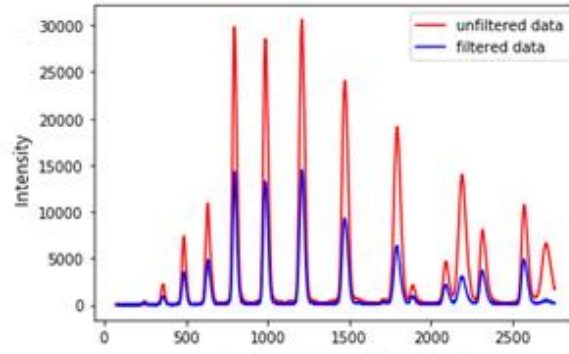
In formula (4) the intensities recorded by the detector for the pulse peaks that interacted with the filter were set as the output intensity. While the intensities recorded by the detector for the impulse that did not interact with the filter were chosen as the input intensity.

Having calculated these values of T, they were compared with graph 1 to find the corresponding energy values. However, from graph 1, a theoretical trend is expected for the most energetic peaks which offers a transmission percentage of about 60%. The percentages obtained by the data do not exceed 48%. While no variations with respect to what was expected are recorded for the values of T for the less energetic harmonics.

This phenomenon could be explained by noting that when the light pulse hits the aluminum filter, the more energetic harmonics can cause oxidation of the material, creating a thin Al_2O_3 patina. Therefore, in the transmission spectrum, it was as if the light beam first passed through one material and then the other. In fact, by performing a combination between the transmission curves of aluminum and Al_2O_3 a curve is obtained that presents a sharp fall in the range of energies corresponding to the most energetic peaks and thus explaining the values other than 60% previously estimated expectation.



Graph 1: transmission spectrum for a specific thickness of an aluminium sample (source: [Filter Transmission \(lbl.gov\)](#))



Graph 2: Overlay of Graphs 1 and 2 for m=1.

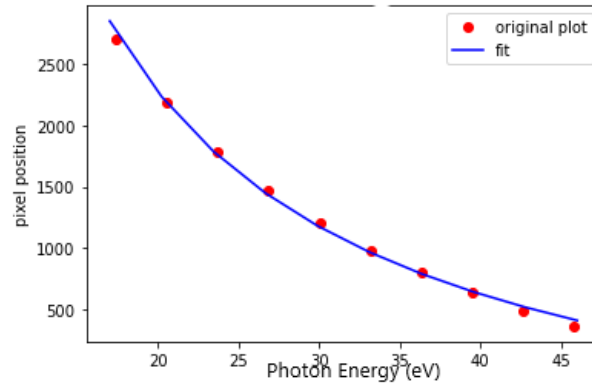
Subsequently, the harmonics were determined by calculating different energy values, using the following relationship:

$$E = nE_0$$

Where n is the number of the harmonic and E is obtained as the n-th multiple of the fundamental energy. Starting from different values of n and comparing the energies obtained with those estimated from the Aluminum transmission spectrum.

In conclusion, the conversion relationship between pixel and energy is then determined in order to represent the data sets obtained by the detector as a function of intensity and energy.

Therefore, the plot shown in graph 3 is obtained.



Graph 3: experimental points fitted with relation (1) inherent to the pixel vs energy plot.

The fit was then performed on this trend of the experimental points (red) using the relation (3) and the parameters shown in table 6 were found.

The consistency of these data obtained by converting L into units of length was verified.

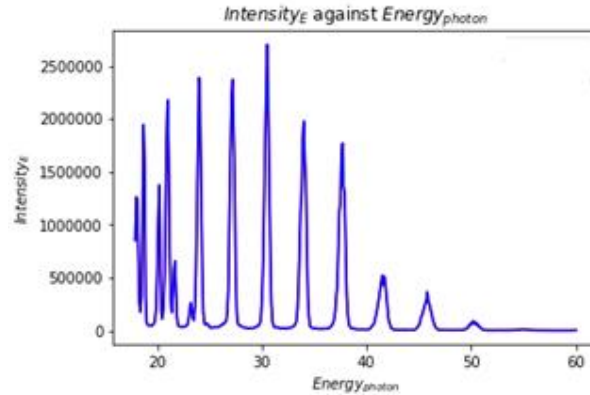
To perform this conversion, the pixel size was obtained from:

$$L(m) = (0.02190 \left(\frac{mm}{pixel} \right)) L(pixel) = 538mm.$$

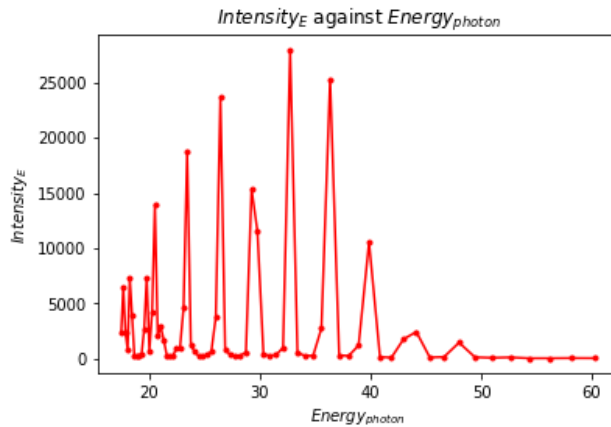
Looking at the given picture of the experimental apparatus the L value was estimated to be between 400mm and 600mm so the value obtained is compatibly acceptable.

Finally, the conversion into energy of the pixels continued, to obtain intensity as a function of energy. In order to carry out this conversion, however, it is necessary to take into account the non-linear relation (3), as can also be seen from graph 2. This non-linearity causes an error in the conversion from pixel to energy, distorting some sections of the final graph.

A computational method was therefore used to overcome this problem. The pixels corresponding to the peak energies found in graph 1 were found. Then, these pixel values were converted into energy values using relation (3) and to overcome the distortion problem we used the loop present in the appendix (I) which is responsible for calculating the average intensity between two pixels limit values and assigning it to the limited bin between the corresponding energy limit values. In this way it was sure to obtain an undistorted and well placed graph (graph 4).



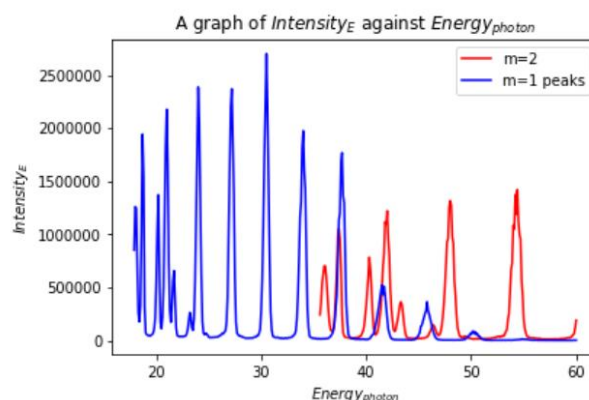
Graph 4: plot of intensity as a function of energy following the computational loop.



Graph 5: graph that is obtained if no correction is made in the conversion of pixels into intensity (only some points have been selected).

In graph 5 there is an evident non-homogeneous spacing between the elements on the energy axis. A representation has been chosen in which the points belonging to the curve have been highlighted and the phenomenon is evident by looking at the difference in spacing between them on the left and on the right.

Finally, the use of order 2 peaks for the equation (1) or (3) was also discussed in order to confirm the calibration. They are much less intense than the peaks corresponding to $m = 1$, therefore there are problems inherent in their captability by the detector (limited by its sensitivity) and in disruption of the measurement. A graph was made in which the intensity vs energy graphs of the two orders were superimposed and it was noted that it was exactly the trend of the original data set with intensity vs pixel, in particular the presence of additional peaks that were ignored in the first analysis was noted (graph 6).



Graph 6: superposition of the graphs inherent to $m = 1$ and $m = 2$ obtained after the conversion of the pixels into energies.

It was also discussed how to find the minimum duration of the impulse using a Fourier transform starting from the amplitude values (frequency dependent) obtained by calculating for each harmonic the square root of the intensity values.

In conclusion, further inaccuracies on the determination of the fit parameters may also have been committed due to phenomena not foreseen in the experimental apparatus. It is therefore necessary to conduct further investigations by conducting additional experiments.

2 Mass Spectrometry

2.1 Introduction

Ionization process

For this experiment ionized molecules by absorbing (one or more) photons with enough energy to separate an electron from them were used. Ionization refers to the process by which neutral atoms or molecules acquire or lose electrons and become ions.

The detecting process uses a spectrometer shown in figure 4.

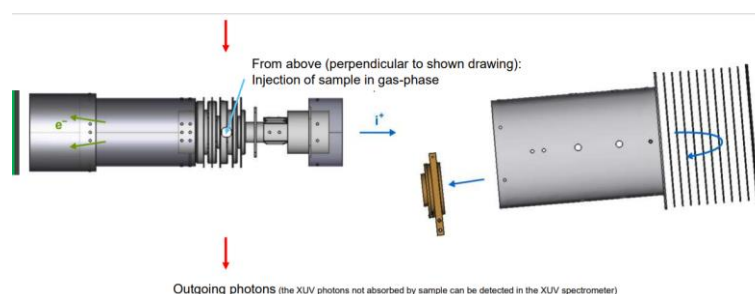


Figure 4: detector structure. The sample to be analyzed is placed in a hole through the grey (metallic) electrode tubes. The sample is sprayed as a gas through this hole. The sample is then crossed by an electromagnetic radiation which ionizes some of its molecules (based on the energy of the incident photons). Therefore, ions are created which are then made to interact with an electric field. This electric field follows the geometry of the electric field between two electrodes of a capacitor and is therefore uniform. We will assume the zone of interaction between ion and electric field of linear type. (E. Månsson, Lecture for DESY Summer Student Program 2021(personal communication))[2].

Having assumed the zone of interaction between the electric field and the linear type ions, it is possible to derive the following equation that connects the total travel time of the distance between the ionization zone and the detector by the ion and its mass (9). The detector will therefore record the various instants the ions will reach and using these times it will be possible to identify the various molecules, as they are directly proportional to the individual masses. In addition, due to this direct proportionality, there is also the certainty that the molecules detected at greater times have greater masses.

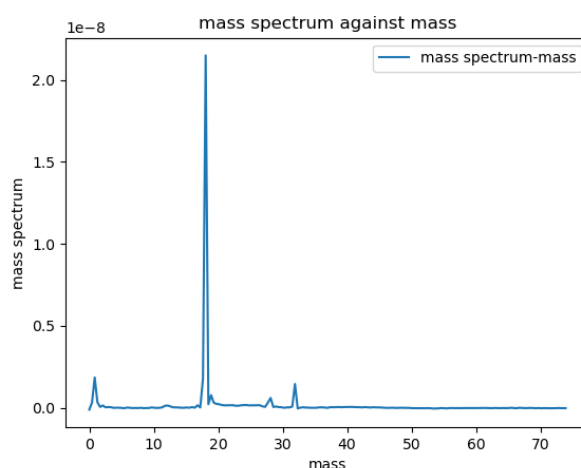
$$t_{tot} = \sqrt{\frac{m}{q}} \left(\sqrt{\frac{2D}{E}} + \frac{L}{\sqrt{2DE}} \right) \quad (9)$$

The demonstration of this relationship is given in the appendix (III).

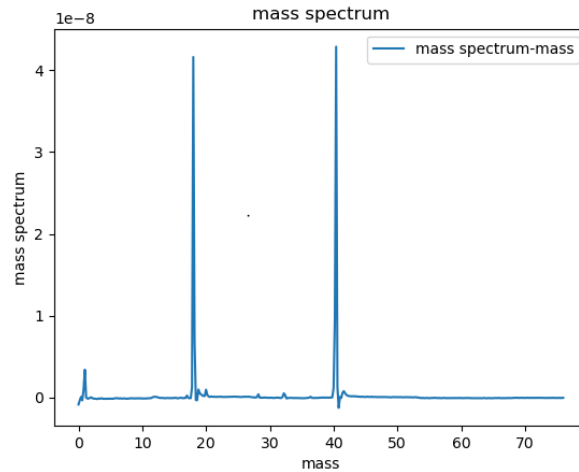
2.2 Data Analysis

A series of samples were analyzed using the device shown in the previous section. First, an air sample was analyzed and the calibration process was taken to obtain from the representation over time, the mass spectrum of the data collected by the detector.

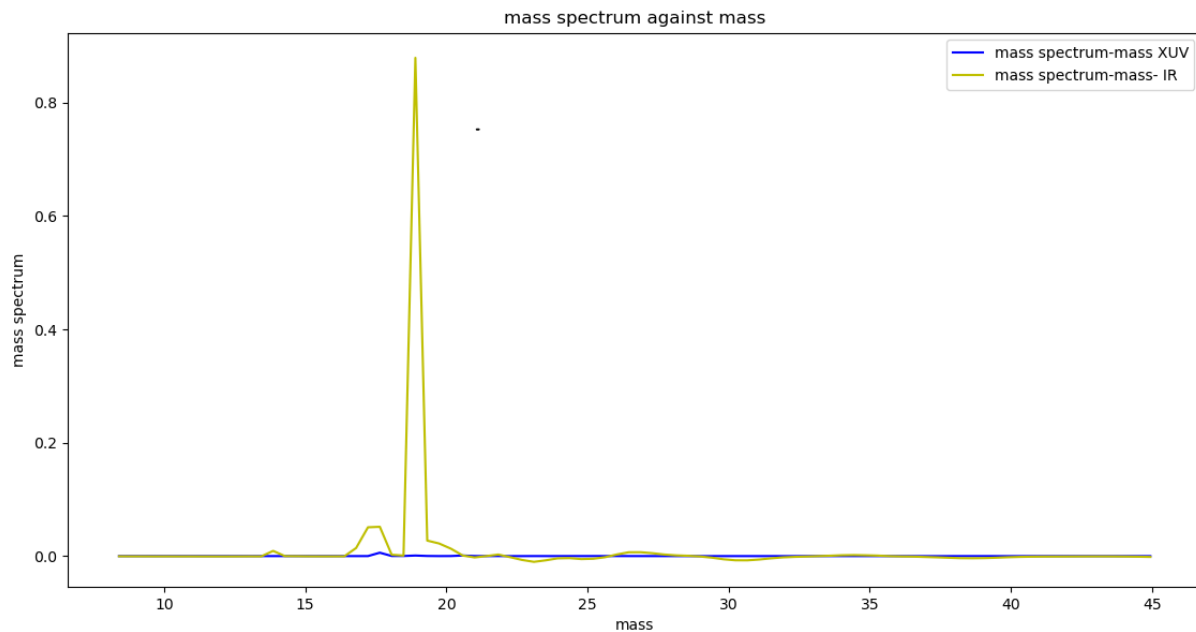
We then continued to recognize an unknown sample and 3 liquids (for which data on ionizations were also provided using different photon energies). Following the analysis on a sample of air using different types of light, it was easy to understand how to determine liquids using this spectroscopic method. The results are shown below and the calibration code is shown in appendix (IV).



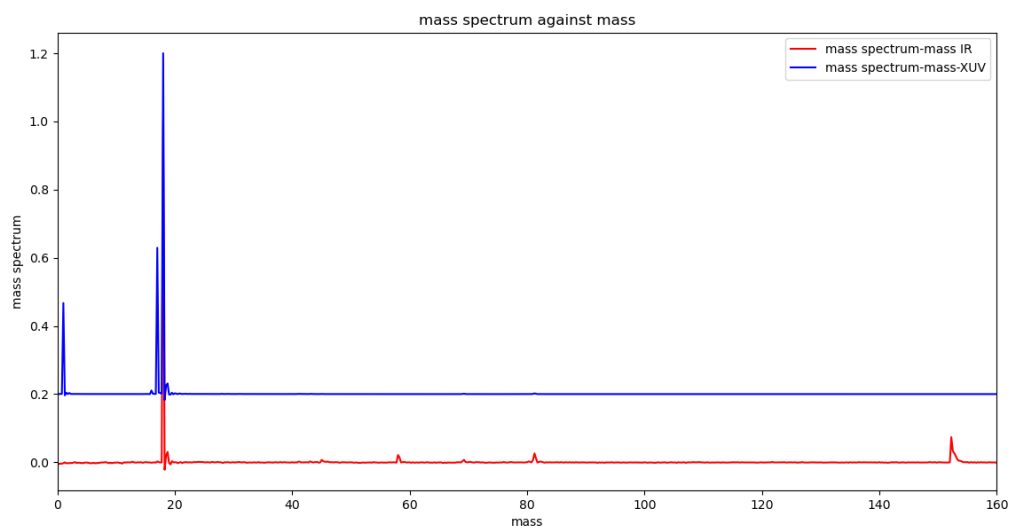
Graph 7: converted spectrum for air. The spectroscopy analysis has highlighted a significant presence of the molecule with a mass of 18 u and which has therefore been identified as water. The next, smaller peaks are the other components of the gas. Their intensity depends on how much these molecules can be ionized by the incident radiation. In this case it is IR and therefore the molecule that manages to be mainly ionized by this radiation is water (also because nitrogen is the gas most present in the air and here it has a very small peak).



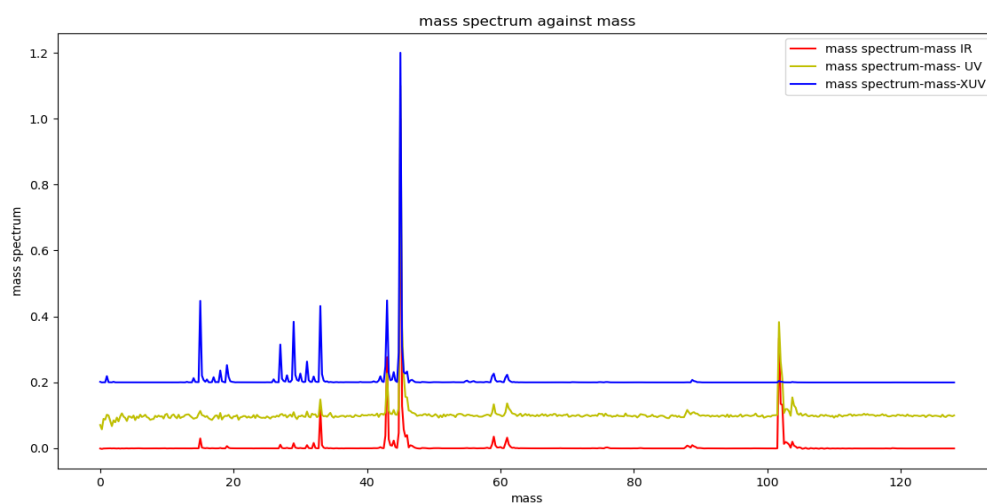
Graph 8: mass spectrum unknown sample. Thanks to this elaboration it has been identified as air and argon. Only the water peak is visible on this spectrum since IR has been used.



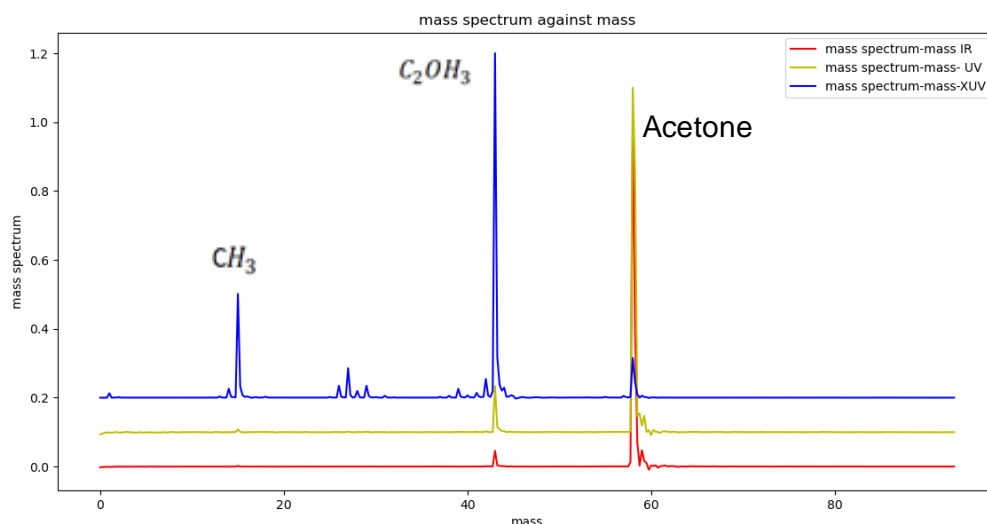
Graph 9: This graph shows the mass spectrum due to the ionization of the air to underline how using different photon energies it is possible to detect the molecules contained in a fluid in a different way with peaks of different intensity. Therefore, the ionization process and consequent identification of the fluid used is strongly dependent on the type of light used. This can be linked to the fact that, to obtain maximum identification, the use of photons of different energy is recommended. In addition, the use of different photons also allows to determine the presence of any residual "dirt" molecules from previous uses (IR for residual organic molecules).



Graph 10: unknown liquid 1 with overlapping IR (red) and XUV (blue). This graph shows the mass spectrum for sample 1 of the liquids used for both IR and XUV. As it can be seen, the most relevant peak is the one corresponding to water. Lower peaks were also recorded corresponding to fragment ions obtained from the ionization of this molecule including H and OH and other organic contaminants.



Graph 11: sample 2 with IR (red), UV (yellow), XUV (blue). This graph shows the mass spectrum corresponding to the ionization of sample 2 for use of IR, UV and XUV. The spectrum appears very varied and it is also very evident that for some molecules the ionization occurs only for certain photon energies. The main peaks allowed us to identify the liquid as lactic acid methyl ester, plus other molecules corresponding to ionization products.



Graph 12: this graph shows the mass spectrum corresponding to sample 3 for the photon energies IR (red), UV (yellow) and XUV (blue). The major peak allowed us to identify the liquid as acetone, combined with other ionization fragments such as CH_3 and CH_3O . The fact that only certain types of light can “see” certain molecules is shown here too, in fact the acetone molecule is not well ionized by the XUV (lower peak than the ones for the IR and UV) and the smaller fragments can only be “seen” by the XUV.

Part of the code used for this calibration is shown in Appendix (IV). It should be emphasized that for the calibrations the peaks obtained from the graphs over time corresponding to XUV photon energy have been used. Precisely because XUV ionizes atoms and lighter molecules and offers a more accurate calibration.

3 Velocity Map Imaging (VMI) Spectrometry

3.1 Introduction

For this last task the VMI spectrometry was used, so the starting speed of the ions into the electric field which is into the spectrometer can also be different from zero.

Lensing Effect

This is a phenomenon linked to the internal structure of the spectrometer used. In particular, by choosing the right potential differences between the electrodes (determined using computer simulations) it is possible to make sure that if ions with equal velocity along the vertical axis cross the field thus generated, the dependence on the initial (vertical) position is deleted. For zero initial velocity, we see a single spot on detector in VMI-mode.

3.2 Data Analysis

We are dealing with a spectrometer which is similar to the one of the task two, except that now the electric field is no longer like the one between two expansions of a capacitor, but can be modified in such a way that particles of initial horizontal velocity different from zero and equal, any both their initial vertical position, are focused on the same point. For reasons of symmetry, therefore, at the

end circles of different radii will be seen on the screen, each corresponding to an initial horizontal speed. Furthermore, the faster a particle is, the more it will be deviated from the field (Lorentz force) and therefore the greater radii will correspond to a greater kinetic energy. Hence the proportionality: $r^2 \propto E_c$.

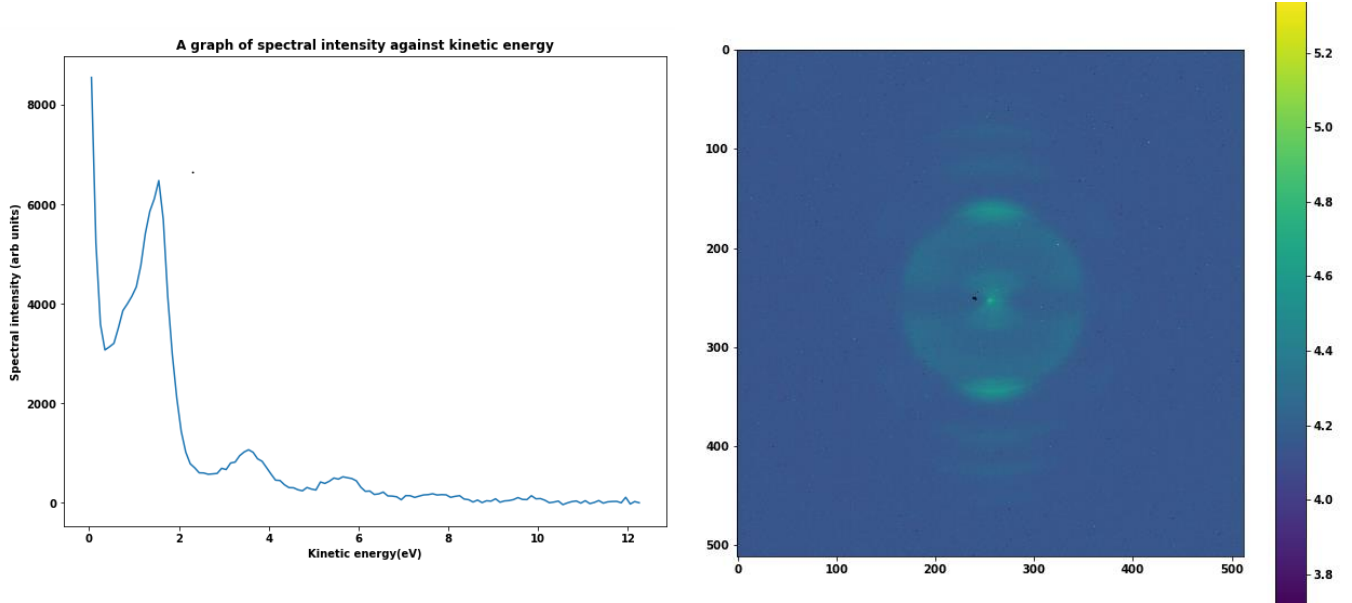


Figure 5: Graphs corresponding to the IR-irradiated Xe sample. On the right, the colormap of the data viewed from the screen. On the left, the graph of the signal compared to the kinetic energy.

As shown in figure 5, it is also possible to verify how, between the various circles, the kinetic energies vary on a regular basis. For this sample of Xe irradiated by IR we expect 1.7 eV and in fact if we look at the distance between the peaks of the graph on the left, we find the confirmation.

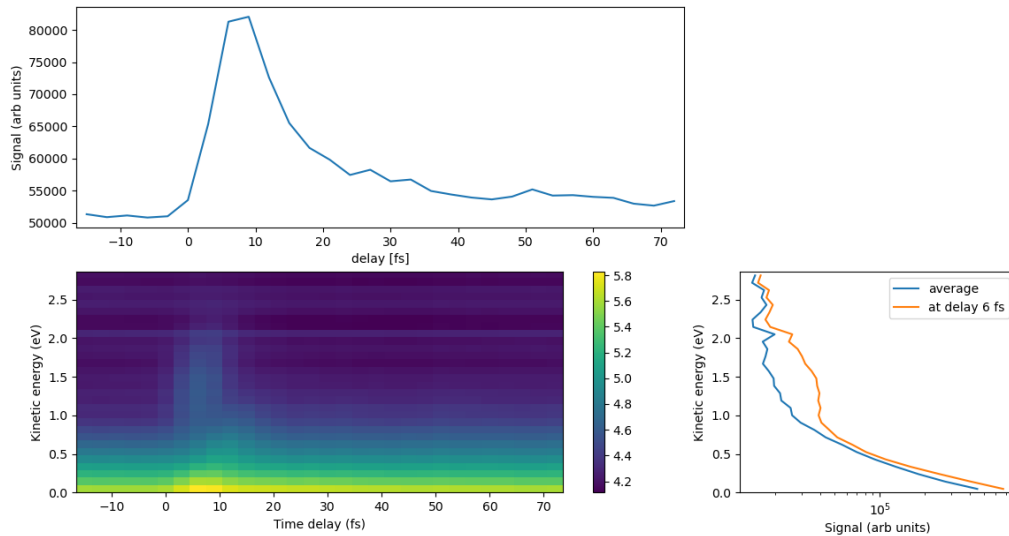


Figure 6: Data representation for the sample of acetone irradiated by UV and IR. Above, the graph showing the signal versus the delay. Bottom right is the graph showing the kinetic energy with respect to the signal. Bottom left is the graph obtained following the computational loop, joining together different data files.

These are the images obtained following a computational method consisting of a for loop for which various files were taken and placed one after the other to obtain the images in figure 6 (appendix (V)). The first thing that can be noticed is the presence of many light stripes also in the upper area of the lower left image. These light stripes are related to systematic background noise of the apparatus for data collection. For this experiment, then, both IR and UV were used and it may happen that these do not reach the sample at the same exact instant of time. The closer they are to each other, the greater the energy response will be. Our sample is acetone and for it the ionization energy is about 9.7 eV. So if three photons (one IR and two UV) were used for this non-linear process, after summing the related photon energies and subtracting the ionization energy for this sample, the final kinetic energy was obtained. The kinetic energy was about 2 eV and this could also be verified looking at the bottom right graph in figure 6. Finally, from the top graph in figure 6, it can be also deduced that the offset for the ionization was 6 fs.

4 Conclusions for the experience

In this experience at the DESY 2021 Summer School many new techniques of data representation and analysis, as well as understanding the research activity carried out by the CFEL-atto group were shown and learnt. Specifically, from the task one a series of experimental and non-experimental phenomena were highlighted, related to the type of experiment conducted.

First of all, the ways of using the spectral transition curve of a filter to help assign and calibrate the harmonics photon energies were explored. Weak points of this transmission comparison technique have also been highlighted and possible solutions have been worked out. In particular, it was suspected the probable formation of aluminium oxide on the filter that dirties the data perceived by the detector. Then, a methodology was developed to be able to move from an intensity as a function of pixels (horizontal position) to an intensity as a function of energy. This process has led to the correct conversion of the pixels into energy, however it still presents some small problems. In fact, the parameter d is very high and therefore not perfectly compatible with the dimensions estimated in the laboratory. Slightly higher than the estimated value, it is also L . Further inaccuracies may also have been due to phenomena not foreseen in the experimental apparatus. It is therefore necessary to conduct further investigations by conducting further experiments.

As regards the second task, methods of analysis and representation aimed at identifying samples used in the laboratory have been assimilated. It was seen how to code a calibration and the creation of mass spectra. From these graphs it was possible to identify the component molecules of each sample provided and using different types of ionizing light it was also highlighted that selected the photon energy, it is not able to ionize every molecule present in the sample. It was therefore concluded that, in order to try to ionize and identify as many elements of the samples as possible, it is advisable to use light of different wavelengths. It is important to underline that this method also allows to highlight contaminant molecules or residues of previous ionizations belonging to previous experiments with different samples that could disturb the measurement.

In conclusion, as concerns the third and last task, the field of VMI imaging was explored and it was studied how to write a code that would allow the correct representation of the provided data, doing the calibration of the electron spectrometer. It was also seen how the harmonics can actually be found starting from the kinetic energy graph in figure 5.

5 Appendix

- I. The computational loop used for converting the graph from intensity (pixel) to intensity (energy):

```
#cicle:
for i in range(len(pos_lims)-1):
    xlow=int(pos_lims[i]) #first included
    xhigh=int(pos_lims[i+1]) + 1 #after last included - +1 so xhigh is included in the range (alternatively, could +1 xhigh i
    if xlow < 0:
        continue #keep running, just ignore this iteration = "continue"
    if xhigh > len(y_list):
        continue

    summ = 0
    for j in range(xlow,xhigh):
        summ=summ + y_list[j]
    integral=summ*1 #pixel width = 1 px
    intensities[i] = integral / E_spacing #here we're getting the spectral intensity in the output spectrum

#creates the array containing intensities from this process
```

- II. Proof of the formula (3)

$$\begin{cases} d\sin\theta_i - d\sin\theta_m = m\lambda \\ \tan\theta_m = \frac{L}{y} \\ \lambda = \frac{hc}{E} \end{cases}$$

$$A = d\sin\theta_i \text{ so}$$

$$\sin\theta_m = \sin\theta_i - \frac{mhc}{dE};$$

$$y = \frac{L}{\tan\theta_m} \text{ so}$$

$$y = \frac{L}{\tan(\arcsin((\frac{1}{d})(A - \frac{mhc}{E}))} .$$

- III. Equation demonstration (1).

For the motion of a charge in an electric field such as that between two expansions of a capacitor we have that:

$$\mathbf{F} = q\mathbf{E}$$

The detector has a first zone in which there is an electric field and a second zone in which no potential difference is applied. In both areas, the vacuum has been created.

Zone 1:

$a = \frac{F}{m} = \frac{qE}{m}$ where $E = \frac{U}{2D}$ is the energy, U is the applied potential difference and D is the distance traveled by the ion in the field, m is the mass of the ion and q is its charge.

For the hourly equation of uniformly accelerated motion:

$$\begin{cases} S_1 = D = \frac{1}{2} \frac{qE}{m} t_1^2 \\ a = \frac{qE}{m} \\ v_1 = at_1 \end{cases}$$

then

$$D = \frac{qEt_1^2}{2m}$$

and

$$t_1 = \sqrt{\frac{2Dm}{qE}} .$$

Zone 2:

$v_1 = cost$ since there is no force field and using the hourly equation for uniform rectilinear motion $S_2 = L = v_1 t_2$

So

$$t_2 = \sqrt{\frac{mL^2}{2qEU}}$$

Where L is the distance traveled by the ion before meeting the detector.

And then, finally: $t_{tot} = t_1 + t_2$.

IV. Calibration code for the different samples:

```
#air calibration:
c = MassCalibration.from_assignments([11.26, 38.37, 40.68], [1, 28, 32], 1E-6)

#unknown gas calibration:
c = MassCalibration.from_assignments([11.4, 30.9, 31], [1, 16, 18], 1E-6)

#unknown liquids calibration:
c = MassCalibration.from_assignments([12.156, 17.941, 18.164], [1, 17, 18], 1E-6)
```

V. Below, the code for loop used for task 3:

```
8 import os
9 import h5py
10 import matplotlib.pyplot as plt
11 import numpy as np
12 import pyqtgraph as pg
13 import os
14 from image_processing import PolarTransform
15
16
17 f=h5py.File('006_01cyc -15.00fs.h5','r')
18 pg.setConfigOptions(imageAxisOrder='row-major')
19
20 img_cal = f['data/accumulated_image'][:]
21 plt.imshow(img_cal)
22 plt.colorbar()
23
24 tr = PolarTransform(img_cal.shape, central_column=82.00, central_row=128.99, angular_bin_width=360,
25                    spectrometer_energy_calibration=21.40*10**-3, pixel_size_xy=0.14914)
26
27 path = os.getcwd() #cwd = current directory
28 chosen_delay = 6 #[fs]
29
30 dir_list = os.listdir(path)
31
32 dir_list = [i for i in dir_list if ".h5" in i] #list of the '.h5' files
33 #print("dir_list len", len(dir_list))
34 #the above for loop is to make sure only the 'h5' files are included in the list
35
36 spectra = np.full((len(tr.energy_abscissa), len(dir_list)), np.nan)
37
38 delays = np.full(len(dir_list), np.nan)
39 #creates a 1D array for the time delay values calculated later
40
41 for i in range(len(dir_list)):
42     f=h5py.File(str(dir_list[i]), 'r')
43     #read the image
44
45     img = f['data/accumulated_image'][:]
46
47     polar_density = tr.transform(img, divide=True) # 2D position (velocity) density
48     #get a spectrum corresponding to the image
49
50     spectra[:,i] = polar_density[:, 0]
51     #use the index to put the spectrum into the array
52     # we want to update all of the rows for column i
53
54     delays[i] = dir_list[i].split(' ')[-1][:-5] #working
55     #obtain the delay number from the file name and put it into an array ^^
```

5 References

[1] M. Nisoli, P. Decleva, F. Calegari, A. Palacios and F. Martin. "Attosecond electron dynamics in molecules", Chem. Rev. **117**, 10760 (2017);

[2] E. Månsson, Lecture for DESY Summer Student Program 2021 (personal communication);

